J Solid State Electrochem (2011) 15:1927–1934
DOI 10.1007/s10008-010-1213-7

ORIGINAL PAPER

Evolution of an iron passive film in a borate buffer solution (pH 8.4)

Luis A. Toledo-Matos · Maximo Antonio Pech-Canul

Received: 15 June 2010 / Revised: 1 October 2010 / Accepted: 4 October 2010 / Published online: 19 October 2010

Abstract The evolution under open-circuit conditions of iron passive films formed at 0.8 V_{SCE} in a borate buffer solution at pH 8.4 was investigated with electrochemical impedance spectroscopy (EIS) and cyclic voltammetry. The composition of the freshly formed passive film as determined by X-ray photoelectron spectroscopy (XPS) was found to be in agreement with a bilayer model, where the inner layer is composed mainly of iron oxide and the outer layer consists of a hydrated material. Results of XPS measurements also showed that the open-circuit breakdown of passive films was consistent with a reductive dissolution mechanism. When the iron electrode reached an intermediate stage in the open-circuit potential decay (approximately −0.3 V_{SCE}), the oxide film, containing both Fe(II) and Fe(III), was still protective. The impedance response in this stage exhibited a mixed control by charge transfer at the metal/film and film/solution interfaces and diffusion of point defects through the film. At the final stage of the open-circuit potential decay (approximately −0.7 V_{SCE}), the oxide film was very thin, and the ratio of Fe^{3+}/Fe^{2+} and O^{2-}/OH^{-} had decreased significantly. The impedance response also exhibited a mixed charge-transfer–diffusion control, but the diffusion process was related to transport of species in the electrolyte solution resulting from dissolution of the oxide film.

Keywords Passive films · Borates · Open-circuit · Breakdown

L. A. Toledo-Matos · M. A. Pech-Canul (✉)
Departamento de Física Aplicada, CINVESTAV-Mérida,
Km. 6 Ant. Carr. a Progreso, AP 73 Cordemex,
CP 97310 Mérida, Yucatan, Mexico
e-mail: max@mda.cinvestav.mx

Introduction

The structure and composition of the passive film on iron in borate buffer solution at pH 8.4 have been investigated for several decades. Early work by Nagayama and Cohen suggested that the passive film is composed of an inner Fe_3O_4 and an outer γ-Fe_2O_3 layer [1, 2]. Cahan and Chen proposed that the passive film consists of a continuous array of oxide ions with a gradient in average valency and occupancy of interstitial sites [3]. M.E. Brett et al. have indicated that the passive film on iron resembles a γ-Fe_2O_3-like oxide when the solution is free from Fe^{2+} ions and γ-FeOOH when such ions are present [4]. By application of in situ X-ray absorption near-edge spectroscopy (XANES), it was found by other researchers that the passive film can be described as a mixed oxidation state iron oxide containing primarily Fe^{3+} ions, having amorphous or spinel structure (similar to γ-Fe_2O_3 or Fe_3O_4) [5, 6]. In recent publications, other authors support the duplex model, but suggesting that it consists of an outer layer mostly of iron hydroxide and an inner layer of iron oxide [7–10]. While there is still disagreement about the crystallographic structure and the composition of the passive film on iron, it is generally agreed that the passivity of iron is primarily due to the inner barrier layer, although the outer layer modifies the electrochemical response of the interface [11].

It is well known that the passive film, once formed, is not an inert layer, but instead is a system in dynamic equilibrium between growth and dissolution [12, 13], such that concerns about its reactivity and stability are also important [14, 15]. In the context of studies aimed at elucidating the nature and stability of the passive oxide film on Fe, some authors have used galvanostatic cathodic reduction [16–18] and open-circuit breakdown experiments [16, 19]. It is commonly observed from potential

decay curves that the open-circuit potential decreases to a value in the active region of iron a certain time after the formation potential is switched off, and such behavior has been interpreted in terms of dissolution of the passive film through chemical and electrochemical effects [19]. Recently H. Deng et al. have used open-circuit breakdown experiments to study the reconstruction process in air of iron passive films formed in a borate buffer solution at pH 8.4 [20] and to investigate the evolution in borate solution of air-formed films [21]. In this study, iron passive films were formed at 0.8 V_{SCE} in a pH 8.4 borate buffer solution, and the open-circuit potential decay was recorded under de-aerated conditions. The objective was to identify changes in surface composition using X-ray photoelectron spectroscopy (XPS) at different stages of the potential decay and to correlate the observations with the corresponding electrochemical impedance response and cyclic voltammogram.

Experimental

All experiments were carried out in a three-electrode electrochemical cell with a platinum foil as a counter electrode and a saturated calomel electrode (SCE) as the reference electrode. The working electrode was made from iron rod (Goodfellow, 99.99%) embedded in epoxy resin leaving an exposed area of 0.78 cm^2. Prior to each measurement, the working surface was abraded down to a 1,200 grit SiC paper and then polished with a diamond suspension to a 1-μm finish. Ultrasonic cleaning with ethanol and distilled water and drying with air followed this process. Experiments were performed at ambient temperature (~22 °C) in borate buffer (0.075 M $Na_2B_4O_7{\cdot}10H_2O$, 0.3 M H_3BO_3, pH 8.4). The solutions were prepared from reagent-grade chemicals and distilled water. Prior to and during all the experiments, the electrolyte was purged with pure nitrogen.

For all electrochemical tests, a Gamry series G300 potentiostat–galvanostat was used. The iron electrode was initially reduced potentiostatically at −1 V_{SCE} for 5 min to remove the air-formed oxide film. In order to find the potential range where passive behavior is observed, a potentiodynamic polarization was carried out at a sweep rate of 1 mV s^{-1}. It was found (Fig. 1) that the electrode was passive in the potential range between −0.2 and 0.9 V_{SCE}, with a pseudo-steady state current density of roughly 2 μA cm^{-2}. Hence, a potential of 0.8 V_{SCE} was chosen to grow passive films for analysis using open-circuit potential (E_{oc}) decay experiments and XPS analysis. The passive electrodes were formed by stepping the potential to 0.8 V_{SCE} for 2 h immediately after the initial cathodic pretreatment.

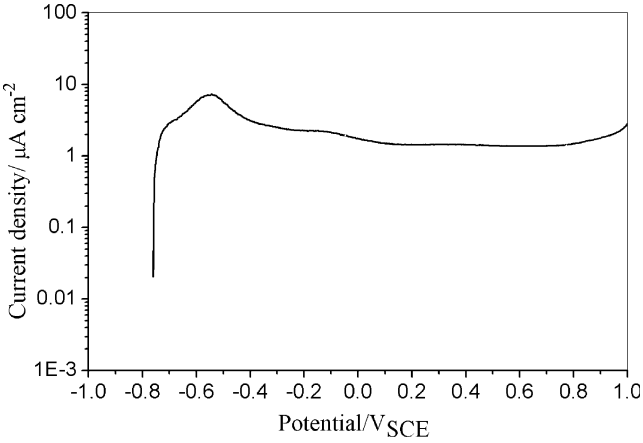

Fig. 1 Anodic polarization curve of iron in borate buffer solution at pH 8.4, recorded at a scan rate of 1 mV s^{-1}

The first set of experiments consisted only in the formation of the passive film at 0. 8 V_{SCE} and then recording E_{oc} for 2 h in the same de-aerated solution. The potential decay resembled that reported by other authors [19–21], with the following features: an abrupt potential drop immediately after the formation potential is switched off, a stage of slow potential decrease, then another abrupt potential drop, and finally a stage of nearly constant potential (presumably corresponding to the active region of iron). In this work, the two stages with nearly constant potential will be referred to as intermediate and final stages of the potential decay.

For the second set of experiments, the passive film was formed during 2 h, then the polarization was switched off and the electrode potential was allowed to evolve freely until it reached the intermediate stage. Since stability conditions were fulfilled, an EIS measurement was carried out applying a ±10 mV sinusoidal signal around the corresponding E_{oc}, with five points per decade in the frequency range 5 kHz–0.05 Hz. Immediately after the EIS measurement, the potential was stepped to −0.9 V_{SCE} and a single sweep cyclic voltammogram was recorded at a scan rate of 10 mV s^{-1}. In the third set of experiments, the passive film was formed at 0.8 V_{SCE}, and after circuit opening, the electrode potential was allowed to evolve freely until it reached the final stage. Again, since stability conditions were fulfilled, an electrochemical impedance measurement was carried out at the corresponding E_{oc}, followed by a single sweep cyclic voltammogram starting at −0.9 V_{SCE}.

In order to elucidate changes in surface composition during open-circuit decay, one sample was withdrawn from the solution immediately after the 2 h potential step at 0.8 V_{SCE} (freshly formed passive film), another sample from the second set of experiments was withdrawn when E_{oc} was in the intermediate stage, and a third sample from

the third set of experiments was withdrawn when its E_{oc} had just reached the final stage. In each case, the sample was rinsed with deionized water, dried with air, and finally transferred to the XPS equipment. XPS analyses were performed with a Perkin-Elmer PHI 560/ESCA-SAM system (equipped with a double-pass cylindrical mirror analyzer with a base pressure of 2×10^{-9} Torr) using Al Kα as the exciting radiation. Argon ion sputtering of the samples was performed for a few seconds with 4 keV energy ions and a 10 μA cm^{-2} current beam (raster size of 5×5 mm) to remove surface contamination. The XPS analyses consisted of (1) a survey spectrum (0–1,000 eV) and (2) high-resolution spectra for Fe 2*p* and O 1*s*. A scanning step of 1 and 0.2 eV/step with an interval of 50 ms was utilized for the survey spectrum and high-resolution spectra, respectively. Binding energy calibration was based on C 1*s* at 284.6 eV. For curve fitting and decomposition, the XPSPEAK software [22] was used, and a simple linear-type background removal was performed on the data. As a fitting strategy for the Fe 2*p* spectrum, the values for spin-orbital splitting and satellite energy shift were constrained to typical values reported in the literature [23–26]. To determine the Fe^{3+}:Fe^{2+} and O^{2-}:OH^{-} ratios, the intensity was defined by the peak area rather than the peak height.

Result and discussion

Relative changes in composition and thickness of passive films during open-circuit potential decay measurements

Figure 2 shows a typical open-circuit decay curve obtained in this work. As indicated above, it resembles that reported by other authors for iron passivated potentiostatically in borate buffer solutions [19, 20]. As pointed out by Li et al. [19], the first potential drop from the formation potential can be ascribed to the IR drop of the passive film while the slow potential decrease, labeled as "intermediate stage" in Fig. 2, is related to dissolution of the passive film and decrease of the amount of iron with higher valence. The "final stage" which corresponds to iron in the active region is attained after a certain period of time, depending on film thickness and the amount of iron atoms of higher valence [19]. Hence, the time period before reaching the final stage is expected to be longer for passive films more resistant to open-circuit breakdown.

In order to evaluate changes in the composition of the film during open-circuit potential decay, the XPS analyses of iron electrode samples in the intermediate and final stages ($E_{oc}\approx-0.3$ V_{SCE} and -0.7 V_{SCE}, respectively) were compared to the XPS analysis for a passive film freshly grown at 0.8 V_{SCE}.

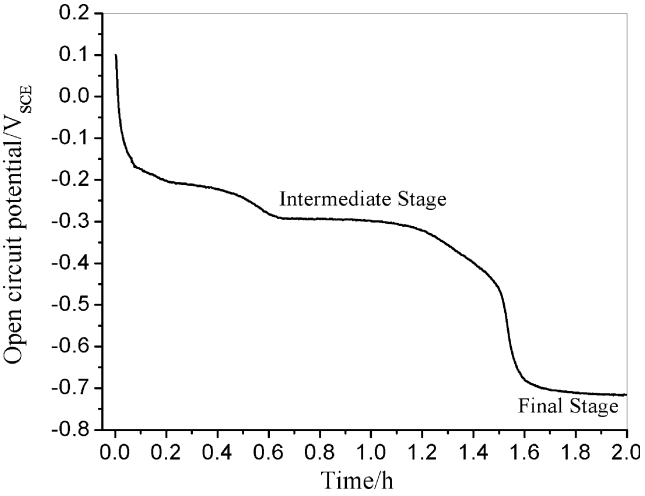

Fig. 2 Potential decay of an iron electrode in the borate buffer solution after 2-h passivation at 0.8 V_{SCE}

Figure 3 shows the high-resolution spectra of Fe 2*p* and O 1*s* for a freshly formed iron passive film in a borate buffer solution pH 8.4. The Fe 2*p* spectrum includes the $2p_{1/2}$ and $2p_{3/2}$ peaks associated to spin-orbit splitting. Results of deconvolution with the XPSPEAK program showed that the Fe 2*p* spectrum contains peaks corresponding to Fe^{2+} and Fe^{3+} plus a satellite structure associated to the $2p_{3/2}$ main peak of Fe^{2+}. Parameters resulting from the curve fit are presented in Table 1. The binding energies for the $2p_{3/2}$ main peaks are consistent with those commonly observed for metallic iron and iron oxides [23–28]. The proportions of Fe^{3+} and Fe^{2+} in Table 1 would appear in principle as an indication that the passive

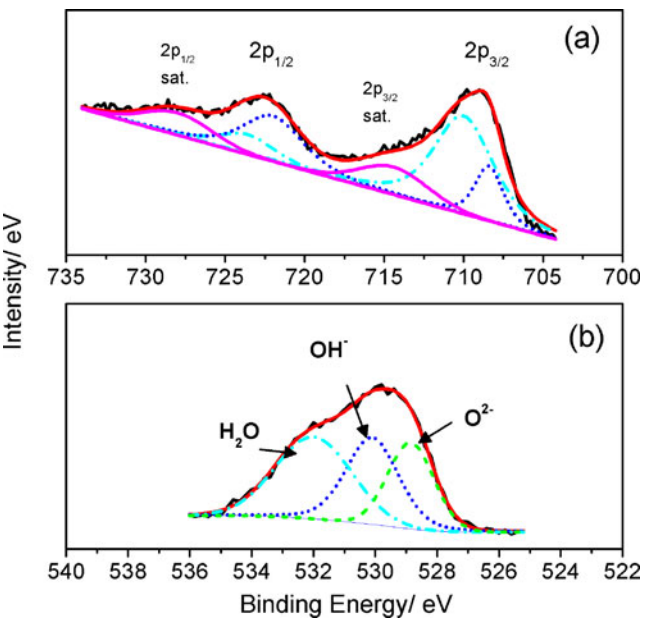

Fig. 3 High-resolution XPS spectra for a freshly grown passive film at 0.8 V_{SCE}. **a** Fe 2*p* and **b** O 1*s*

Table 1 Results of deconvolution of Fe 2*p* spectra in Figs. 3, 4, and 5, including the ratio of intensities for O^{2-} and OH^-

System	Fe 2*p*					O 1*s*
	Peak	B.E. $2p_{3/2}$ (eV)	Δ B.E. [$2p_{1/2}$ −$2p_{3/2}$] (eV)	$2p_{3/2}$ satellite shift	Proportion in $2p_{3/2}$ envelope	O^{2-}/OH^- ratio
Freshly grown passive	Fe^0					
	Fe^{2+}	708.4	13.6	6	0.34	
	Fe^{3+}	710	13.6		0.66	
						0.79
Iron electrode in intermediate stage	Fe^0	706.7	13.2			
	Fe^{2+}	709.8	13.6		0.38	
	Fe^{3+}	711.6	13.6		0.60	
						0.55
Iron electrode in final stage	Fe^0	706	13.2			
	Fe^{2+}	709	13.6	6	0.49	
	Fe^{3+}	710.6	13.6		0.41	
						0.45

film consists of magnetite since for such oxide the Fe^{2+}:Fe^{3+} ratio should be 1:2 or 0.33:0.67; however, deconvolution of the corresponding O 1*s* spectrum (Fig. 3b) suggests that the film is a hydrated layer containing FeOOH since OH^- (from hydrous iron oxides) represents an important contribution (see O^{2-}/OH^- ratio in Table 1). Oblonsky et al. [6] proposed that the passive film can be described as a mixed oxidation state iron oxide containing both Fe^{3+} and Fe^{2+} ions even when it is formed at high potentials. The amount of Fe^{2+} shown in Table 1 is higher than reported in ref. [6], but this may be due to the presence of Fe^{2+} ions in the solution, associated to iron dissolution prior to formation of passive film [4, 6].

Figure 4 shows the high-resolution spectra of Fe 2*p* and O 1*s* regions for an iron electrode withdrawn from the solution when it reached the intermediate stage ($E_{oc} \approx -0.3$ V_{SCE}). Deconvolution of the Fe 2*p* spectrum showed the presence of three peaks, corresponding to metallic iron, Fe^{2+}, and Fe^{3+}. Parameters resulting from the curve fit are presented in Table 1. The binding energies for the $2p_{3/2}$ main peaks are slightly different compared to the ones obtained for the freshly formed passive film, but still within reasonable limits. Analysis of the O 1*s* spectrum showed again the presence of three peaks although that for chemisorbed H_2O decreased. It appears that the film still contained protective oxide or oxyhydroxide from the initial film; however, there was a slight decrease of Fe^{3+} (from 0.66 to 0.6) due to film dissolution. Such dissolution led to a thickness decrease, as suggested by the appearance of the metallic component in the spectrum at a binding energy of 706.7 eV. Table 1 also shows that the O^{2-}/OH^- ratio increased with respect to that for the freshly formed passive film. Hence, at the intermediate stage, the film was not only thinner but also less hydrated than at the beginning of the potential decay. This result is consistent with the bilayer model for the passive film [7–10], where the inner layer mainly consists of iron oxide and the outer layer of iron hydroxide. These results suggest that the outer hydrated layer was partly removed during dissolution.

The Fe 2*p* and O 1*s* spectra obtained for an iron electrode removed from the solution when it reached the final stage of the potential decay ($E_{oc} \approx -0.7$ V_{SCE}) are presented in Fig. 5. Similarly to the results observed for the

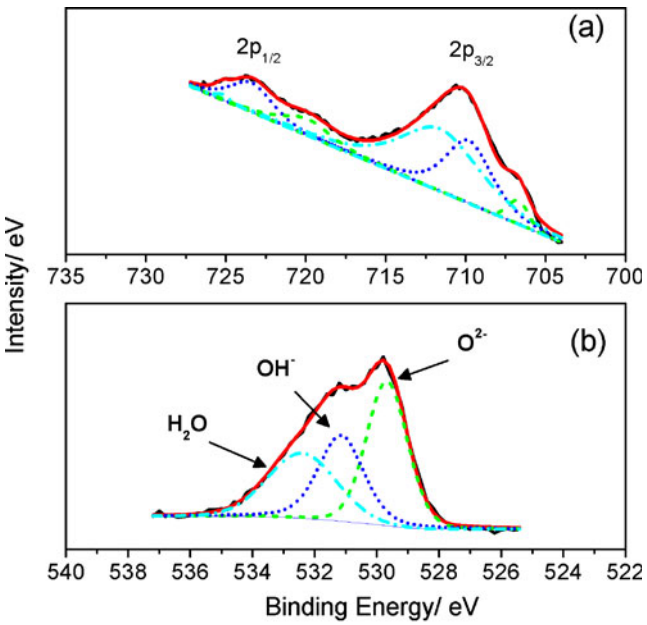

Fig. 4 High-resolution XPS spectra for an iron electrode in the intermediate stage of potential decay (E_{oc}=−0.3 V_{SCE}). **a** Fe 2*p* and **b** O 1*s*

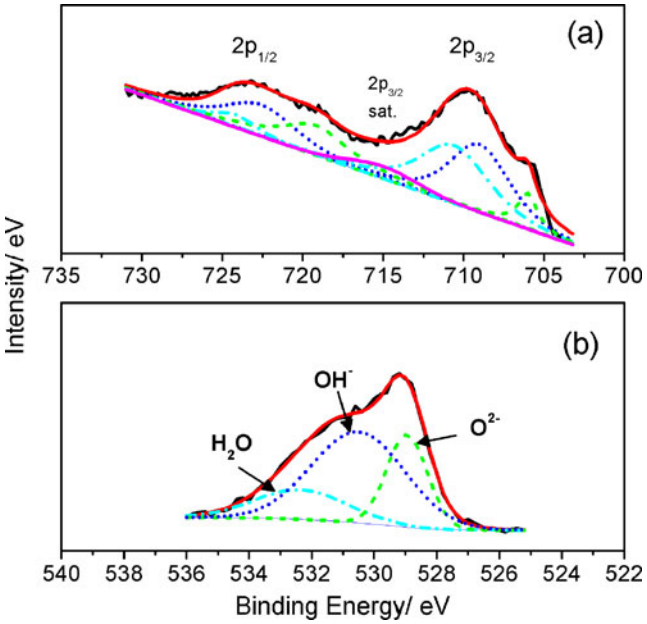

Fig. 5 High-resolution XPS spectra for an iron electrode in the final stage of potential decay (E_{oc}=−0.7 V_{SCE}). **a** Fe 2*p* and **b** O 1*s*

passive film in the intermediate stage, the Fe 2*p* spectrum exhibits contributions of Fe^0, Fe^{2+}, and Fe^{3+}. Considering that individual peaks for O^{2-} and OH^- are observable in the O 1*s* spectrum (apart from the small peak for chemisorbed H_2O), it can be concluded that at the final stage of potential decay (with a potential in the active region) the iron electrode was still covered by a layer. The more pronounced signal for metallic iron indicates that such layer was very thin. As shown in Table 1, a further reduction in the amount of Fe^{3+} occurred (from 0.6 for the film in the intermediate stage to 0.41 for the film in the final stage). It can also be observed that the Fe^{3+}/Fe^{2+} and O^{2-}/OH^- ratios in the final stage are lower than those in the intermediate stage. This suggests that during open-circuit decay, the passive film was dissolved reductively and became less protective. Due to the increased amount of Fe^{2+}, it can be proposed that such thin layer had iron ferrous species constituents such as FeO and $Fe(OH)_2$. While OH^- in the freshly formed passive film was bound to ferric iron, in the thin layer at the end of potential decay, it was bound to ferrous iron.

The increasing intensity of the Fe^0 peak in the Fe 2*p* spectra of Figs. 3, 4, and 5 has a correlation with film thickness which decreased during potential decay. The initial thickness (that for the freshly formed passive film) was expected to be around 3.5 nm, according to results obtained by other authors in the same media and formation potential using a variety of experimental techniques such as coulometry [1], capacitance [11], ellipsometry [29], and Auger electron spectroscopy depth profiling [8]. XPS can also be used to determine oxide film thickness (*d*), according to [30]:

$$d = \lambda_{ox}\sin\theta \ln\left(1 + \frac{N_m\lambda_m I_{ox}}{N_{ox}\lambda_{ox} I_m}\right) \quad (1)$$

where λ_{ox} is the inelastic mean free path of photoelectrons emitted by the Fe $2p_{3/2}$ core level in the oxide, θ is the take-off angle of photoelectrons with respect to the sample surface, N_m and N_{ox} represent the atomic density of atomic iron and atomic density of iron in the oxide, respectively, and *I* represents the intensity (peak area) of the Fe $2p_{3/2}$ photoelectron peaks of metal (subscript m) or oxide (subscript ox). The Fe^0 signal was observed only for the iron electrode in the intermediate and final stages. Values of oxide film thickness were estimated for these two cases using the experimental value of θ=60° and reported values for λ and *N* (λ_m=12.4 Å, N_m=0.141 mol cm^{-3}, λ_{ox}=15.4 Å, and N_{ox}=0.066 mol cm^{-3}) [31]. The values obtained were 4.2 and 3 nm, respectively. They appear higher than the expected (assuming that the initial thickness was around 3.5 nm), but nevertheless they reflect the correct trend of decreasing thickness. An additional indication of relative changes in film thickness was obtained by recording XPS spectra after Ar ion bombardment of the samples for 5 min. Figure 6 shows a comparison of Fe 2*p* spectra for the three samples (freshly formed passive film, iron electrode

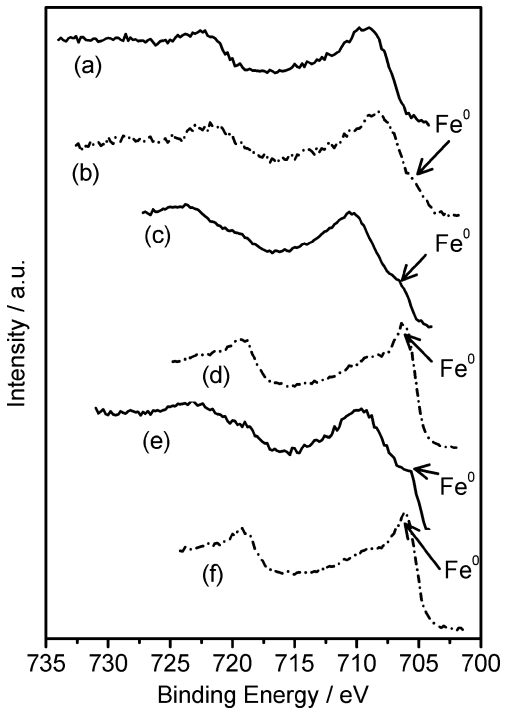

Fig. 6 Comparison of Fe 2*p* spectra for freshly formed passive film (*a*, *b*), an iron electrode in the intermediate stage (*c*, *d*), and an iron electrode in the final stage (*e*, *f*). XPS spectra were recorded at the surface (*solid line*) and after 5-min Ar ion etching (*slash-dotted line*)

withdrawn from solution when E_{oc}=−0.3 V_{SCE} and iron electrode withdrawn from solution when E_{oc}=−0.7 V_{SCE}) obtained under two conditions (unetched and after 5 min etching). In each case, the spectra obtained after etching exhibits a slight shift towards lower binding energy, which can be explained by a reduction of iron species (e.g., from Fe^{3+} to Fe^{2+}) due to the Argon ion sputtering [24]. Accordingly, deconvolution of the spectra obtained after sputtering was not performed because it could lead to misleading parameter values. However, qualitative information can be obtained by comparing relative changes in the Fe^0 component. For the freshly formed passive film, even after sputtering (Fig. 6b) the oxide film thickness was higher than the maximum escape depth of photoelectrons, and the Fe^0 is barely perceptible. For the iron samples withdrawn from solution at the intermediate and final stages of potential decay, the Fe^0 signal was already observable at the surface and increased significantly after sputtering, indicating that the corresponding films were thinner than the initial passive film.

Electrochemical response of films during open-circuit potential decay measurements

Figures 7 and 8 show the impedance spectra obtained at the E_{oc} corresponding to the intermediate and final stages of the potential decay, respectively. Fitting of the experimental data with various equivalent circuit models proposed in the literature [19, 32–34] for passive iron in slightly alkaline solutions was attempted. The best agreement between experiment and fitting was obtained with the equivalent circuit shown in Figs. 7 and 8, similar to the Randles circuit. Such circuit contains a constant phase element

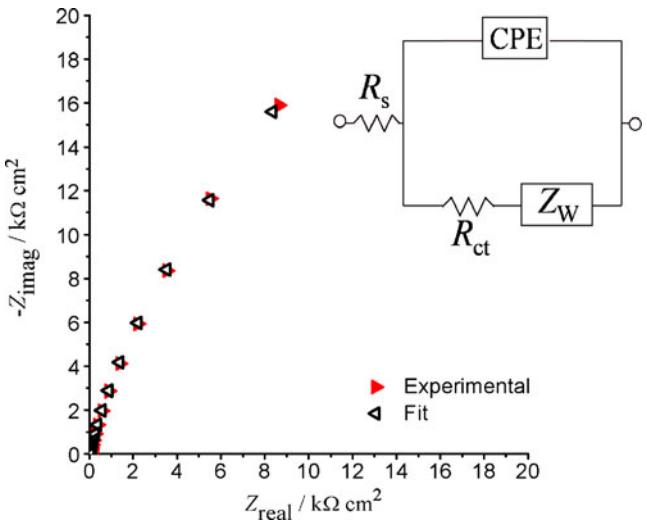

Fig. 7 Complex plane impedance diagrams for an iron electrode in the intermediate stage of the potential decay (E_{oc}=−0.3 V_{SCE}) and the equivalent circuit used to model the data

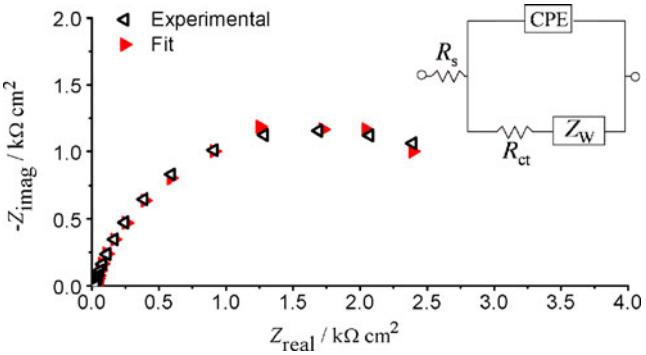

Fig. 8 Complex plane impedance diagrams for an iron electrode in the final stage of the potential decay (E_{oc}=−0.7 V_{SCE}) and the equivalent circuit used to model the data

(CPE), which is usually introduced to account for non-ideal capacitive behavior of the interfacial charge storage mechanism. Its admittance is given by

$$Y_{CPE} = Y_0(j\omega)^{\alpha} \tag{2}$$

where ω is the sine wave modulation angular frequency, Y_0 is the base admittance (with dimensions Ω^{-1} s^{α} cm^{-2}), and α is an empirical exponent ($0 \le \alpha \le 1$) which measures the deviation from the ideal capacitive behavior. In this case, the CPE is associated to the capacity of the passive oxide film, R_s corresponds to the electrolyte resistance, R_{ct} represents the charge-transfer resistance at the two interfaces (metal/film and film/solution), and Z_W is the Warburg impedance [35]

$$Z_W = \sigma(1-j)\omega^{-1/2} \tag{3}$$

where σ is the Warburg coefficient (with dimensions Ω $s^{-1/2}$ cm^2), which for the electroactive diffusing species depends on its diffusion coefficient (D) and concentration (C^*) at the corresponding interface, according to [35]

$$\sigma = \left(\frac{RT}{n^2F^2\sqrt{2}}\right)\left[\frac{1}{C^*\sqrt{D}}\right] \tag{4}$$

where n is the number of electrons transferred and F is Faraday's constant. Numerical values of the fit parameters are reported in Table 2. The general observations are consistent with the above discussion about the nature of the oxide films at different stages of the potential decay. The oxide film at the intermediate stage is more protective than that at the final stage, and hence, the charge-transfer resistance is about one order of magnitude higher. According to Eq. (4), the Warburg coefficient increases when either C^* or the diffusion coefficient decrease. In Table 2 the value of σ for the intermediate stage is about 30 times larger than the one corresponding to the final stage. This is an indication that the diffusion mechanism is different in

Table 2 Parameters from least-squares fit of the equivalent circuit in Figs. 7 and 8 to the corresponding impedance spectrum

Stage of E_{oc} decay	R_s/Ω cm^2	Y_0/Ω^{-1} s$^{\alpha}$ cm^{-2}	α	R_{ct}/kΩ cm^2	σ/kΩ s$^{-1/2}$ cm^2
Intermediate	55	1.7×10^{-4}	0.88	25	9.2
Final	28	2.0×10^{-4}	0.84	2.6	0.29

the two stages of the potential decay. In the intermediate stage, the oxide film is protective and the diffusion process is dominated by the transport of point defects across the film [36]. Since this process corresponds to solid state diffusion, the diffusion coefficient is very low. On the other hand, the oxide film in the final stage is poorly protective. In this case, the diffusion process is most likely related to transport of ionic species away from the electrode as the oxide film is dissolved.

A single cyclic voltammogram was obtained for the iron electrode in each of the selected stages of potential decay after formation of the passive film in the borate buffer solution at pH 8.4. Figure 9 shows the cyclic voltammogram obtained at a sweep rate of 10 mV s^{-1} when the electrode reached the final stage. In agreement with observations by other authors [9, 37, 38] for passive iron in borate buffer solution pH 8.4, it exhibits three peaks. The first peak (I) at −0.51 V_{SCE}, which appeared in the anodic sweep, corresponds to the formation of a monolayer of passive film consisting mainly of Fe^{2+} oxide/hydroxide and is followed by a broad anodic peak (II) at 0.02 V_{SCE} which is associated to the conversion to a Fe^{2+}/Fe^{3+} film (possible magnetite and maghemite). At potentials more positive than 0.2 V_{SCE}, the film becomes primarily an oxyhydroxide (possibly γ-FeOOH). During the reverse sweep, a peak appeared at −0.52 V_{SCE} which corresponds to the inverse process of peak II. At more negative potentials, the current increases due to the simultaneous hydrogen evolution reaction and reduction of the passive film. The presence of peak I suggests, in consistency with results discussed above, that the oxide film was so thin that almost all of it disappeared during cathodic polarization. Figure 10 shows the cyclic voltammogram for the iron electrode in the intermediate stage compared to the one obtained in the final stage. In this case, the current in the anodic sweep is lower than observed in Fig. 9 and only two peaks are observed. The peak in the anodic sweep located at −0.17 V_{SCE} is quite possibly due to the transformation of Fe_3O_4 to α-FeOOH [39], and the peak in the cathodic sweep at −0.42 V_{SCE} corresponds to the inverse process. The fact that the current measured in the anodic sweep is lower than observed when the electrode reached the final stage is in good agreement with results of impedance measurements, illustrating that the oxide film in the intermediate stage was still protective.

Conclusions

The composition of the passive film formed in borate solution at pH 8.4 at 0.8 V_{SCE} is in agreement with a bilayer model, where the inner layer is composed mainly of iron oxide and the outer layer is hydrated. Results of XPS measurements showed that the open-circuit breakdown of passive films was consistent with a reductive dissolution mechanism. When the iron electrode reached an intermediate stage in the open-circuit potential decay (approximately −0.3 V_{SCE}),

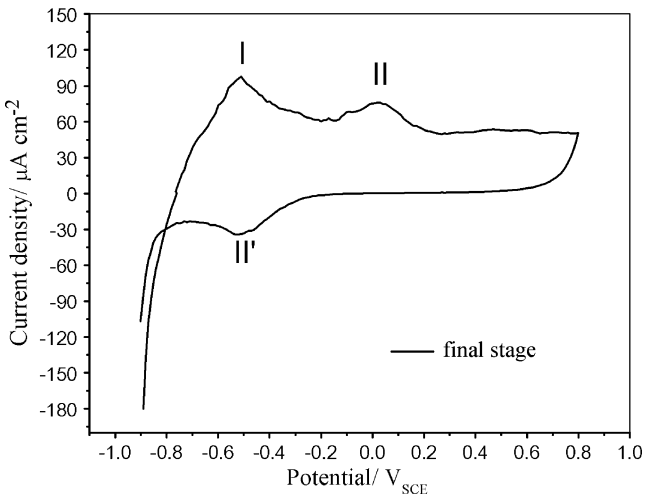

Fig. 9 Cyclic voltammogram obtained for an iron electrode in the final stage of the potential decay (E_{oc}=−0.7 V_{SCE}) recorded at a scan rate of 10 mV s^{-1}

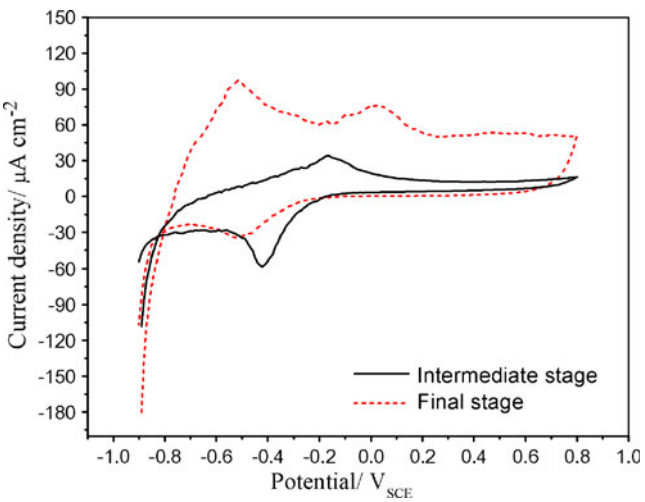

Fig. 10 Cyclic voltammograms obtained for an iron electrode in the two stages of the potential decay recorded at a scan rate of 10 mV s^{-1}

the oxide film, containing both Fe(II) and Fe(III), was still protective. In this stage, the impedance response exhibited a mixed control by charge transfer at the metal/film and film/solution interfaces and diffusion of point defects through the film. At the final stage of the open-circuit potential decay, the oxide film was very thin, and the ratios of Fe^{3+}/Fe^{2+} and O^{2-}/OH^{-} had decreased significantly. In this case, the impedance response also exhibited a mixed charge-transfer–diffusion control, but the diffusion process was related to transport of species resulting from dissolution of the oxide film.

Acknowledgements The authors are grateful to Dr. P. Bartolo Perez and Mr. W. Cauich of CINVESTAV-Mérida for helpful discussions and technical assistance in the XPS measurements. It is also acknowledged the technical assistance of Ms. Marbella Echeverría. Finally, L.A. Toledo Matos is thankful to CONACyT-Mexico for providing a scholarship for his doctoral studies.

References

1. Nagayama M, Cohen M (1962) J Electrochem Soc 109:781–790
2. Nagayama M, Cohen M (1963) J Electrochem Soc 110:670–680
3. Cahan BD, Chen CT (1982) J Electrochem Soc 129:921–925
4. Brett ME, Parkin KM, Graham MJ (1986) J Electrochem Soc 133:2031–2035
5. Davenport AJ, Sansone M (1995) J Electrochem Soc 142:725–730
6. Oblonsky LJ, Davenport AJ, Ryan MP, Isaacs HS, Newman RC (1997) J Electrochem Soc 144:2398–2404
7. Büchler M, Schmuki P, Böhni H (1998) J Electrochem Soc 145:609–614
8. Sieber IV, Hildebrand H, Virtanen S, Schmuki P (2006) Corros Sci 48:3472–3488
9. Díez-Pérez I, Gorostiza P, Sanz F, Müller C (2001) J Electrochem Soc 148:B307–B313
10. Díez-Pérez I, Sanz F, Gorostiza P (2006) Curr Opin Solid State Mater Sci 10:144–152
11. Liu J, Macdonald DD (2001) J Electrochem Soc 148:B425–B430
12. Macdonald DD (1999) Pure Appl Chem 71:951–978
13. Schmuki P (2002) J Solid State Electrochem 6:145–164
14. Schultze JW, Lohrengel MM (2000) Electrochim Acta 45:2499–2513
15. Virtanen S, Schmuki P, Isaacs HS (2002) Electrochim Acta 47:3117–3125
16. Bardwell JA, MacDougall B, Graham MJ (1988) J Electrochem Soc 135:413–418
17. Davenport AJ, Bardwell JA, Vitus CM (1995) J Electrochem Soc 142:721–724
18. Schmuki P, Virtanen S, Davenport AJ, Vitus CM (1996) J Electrochem Soc 143:574–582
19. Li WS, Cai SQ, Luo JL (2004) J Electrochem Soc 151:B220–B226
20. Deng H, Ishikawa I, Yoneya M, Nanjo H (2004) J Phys Chem B 108:9138–9146
21. Deng H, Nanjo H, Qian P, Xia Z, Ishikawa I (2006) Electrochim Acta 52:187–193
22. Kowk RMW (2000) XPSPEAK Version 4.1 XPS Peak Fitting Program. Available at http://www.uksaf.org/software.html. Accessed 30 Sept 2010
23. Grosvenor AP, Kobe BA, Biesinger MC, McIntyre NS (2004) Surf Interface Anal 36:1564–1574
24. Mills P, Sullivan JL (1983) J Phys D 16:723–732
25. Yamashita T, Hayes P (2008) Appl Surf Sci 254:2441–2449
26. Aronniemi M, Sainio J, Lahtinen J (2005) Surf Sci 578:108–123
27. McCaffery E, Bernett MK, Murday JS (1988) Corros Sci 28:559–576
28. Temesghen W, Sherwood PMA (2002) Anal Bioanal Chem 373:601–608
29. Sato N, Cohen M (1964) J Electrochem Soc 111:512–519
30. Strohmeier BR (1990) Surf Interface Anal 15:51–56
31. Frateur I, Carnot A, Zanna S, Marcus P (2006) Appl Surf Sci 252:2757–2769
32. Martini EMA, Muller IL (2000) Corros Sci 42:443–454
33. Hamadou L, Kadr A, Benbrahim N (2005) Appl Surf Sci 252:1510–1519
34. Alves VA, Brett CMA (2002) Electrochim Acta 47:2081–2091
35. MacDonald JR (1987) Impedance Spectroscopy. Wiley, New York
36. Chao CY, Lin LF, Macdonald DD (1982) J Electrochem Soc 129:1874–1879
37. Jovancicevic V, Kainthla RC, Tang Z, Yang B, Bockris JO'M (1987) Langmuir 3:388–395
38. Rubim JC (1993) J Electrochem Soc 140:1601–1606
39. Amaral ST, Martini EMA, Muller IL (2001) Corros Sci 43:853–879